Coherent Control of Light Scattering from Nanostructured Materials by Second-Harmonic Generation

Sergio G. Rodrigo,[1] Hayk Harutyunyan,[1] and Lukas Novotny[1,2]
[1]*Institute of Optics, University of Rochester, Rochester, New York 14627, USA*
[2]*Photonics Laboratory, ETH Zürich, 8093 Zürich, Switzerland*
(Received 9 November 2012; published 25 April 2013)

We introduce an active, all-optical method for controlling the intensity and directionality of light scattering from single nanostructures. The method is based on the coherent interplay between linear light scattering and second-harmonic generation. The intensity and directionality of scattered light can be controlled by the phase delay and the relative angle between excitation beams. We discuss the principle of this coherent control technique and perform numerical model calculations.

DOI: 10.1103/PhysRevLett.110.177405 PACS numbers: 78.67.Bf, 42.65.Ky, 73.20.Mf, 78.20.Bh

Recent advances in nanofabrication and optical characterization of nanostructured materials have paved the way to new technology at the nanoscale [1–4]. Optical nanoantennas emerged as promising optoelectronic devices that enhance the interaction between light and matter [5,6]. For example, directional emission, one of the most characteristic properties of antennas, has been recently demonstrated at optical frequencies with Yagi-Uda antennas made of gold elements [7]. In that work, as in most other antenna designs, the geometrical parameters and the material properties characterize the antenna performance, which defines these antennas as passive devices. In the work presented here we achieve all-optical control of the antenna response by exploiting the nonlinear optical properties of metal nanostructures. The method makes use of second harmonic generation (SHG) [8–15], a process where two photons create a single photon of half the incident wavelength [16].

Because the induced charge distributions at the second-harmonic (SH) and fundamental frequencies have different symmetries, SHG provides access to electromagnetic (EM) modes that cannot be excited by linear scattering (dark modes). As illustrated in Fig. 1, we exploit the coherent interaction between the polarization currents generated by linear scattering and those induced by SHG and demonstrate that the combined charge distribution can be markedly asymmetric, thereby opening up the possibility of controlling the directionality of radiation. Furthermore, it is possible to suppress or enhance certain EM modes, which provides a means to actively control the scattered intensity.

To understand the principle of this coherent control technique we perform a theoretical model calculation based on a combination of the Finite-Difference Time-Domain (FDTD) method [17] and the volume integral equation [18]. While FDTD is used to compute induced polarization currents and optical near fields, the volume integral equation is employed to propagate the near fields into the far field. In FDTD the linear response of gold is described by a Drude-Lorentz model [19], and to calculate the response at the SH frequency, we follow a perturbative approach, for which the intensity of the exciting field is not decreased due to SHG (nondepletion regime). We first perform a linear calculation to determine the EM field at fundamental wavelength, $\mathbf{E}^{(2\lambda)}$. The SH fields are generated simultaneously. The update equations are the same as in the linear case, with the exception that the source is defined by the second-order polarization vector, $\mathbf{P}^{(\lambda)}$, instead of the incident field. In centrosymmetric materials like polycrystalline metals, the induced polarization at the SH frequency has multiple origins: (i) a dipolar contribution, which is nonzero at material boundaries, and (ii) a quadrupolar contribution, which can be enhanced by surface roughness and nanostructuring [20,21]. Both contributions are of the same order of magnitude, originating from a surface contribution that can be expressed as

$$\begin{aligned}\mathbf{P}_n^{(\lambda)} &= [\chi_{nnn}^{(2)}(E_n^{(2\lambda)})^2 + \chi_{ntt}^{(2)}(E_t^{(2\lambda)})^2]\mathbf{n} \\ \mathbf{P}_t^{(\lambda)} &= 2\chi_{tnt}^{(2)}E_n^{(2\lambda)}\mathbf{E}_t^{(2\lambda)}\end{aligned} \tag{1}$$

where n and t stand for normal and tangential to the surface respectively, and χ_{ijk} are the nonvanishing components of the second-order susceptibility tensor. For gold at a wavelength of 1064 nm we choose $\chi_{nnn}^{(2)} = 250.0$, $\chi_{tnt}^{(2)} = 3.6$,

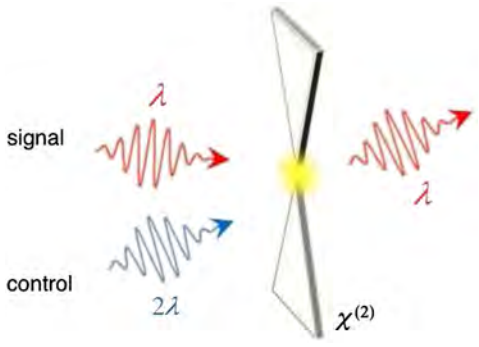

FIG. 1 (color online). Principle of the coherent control method. The scattered intensity and direction of a signal beam is influenced by a control beam of twice the wavelength.

and $\chi^{(2)}_{ntt} = 1.0$ in units of 3.27×10^{-15} cm/V [22]. Pure bulk nonlinearities are negligible compared to surface nonlinearities [13,22]. Furthermore, the inclusion of bulk contributions would not lead to the excitation of new modes and therefore not affect our symmetry considerations. Our code has been tested against analytical results and proven to yield correct results (not shown) [23].

To simplify our calculations we chose a cylindrical symmetry (infinite gold nanowire) and p-polarized fields. The problem can then be treated by a two-dimensional FDTD code. This choice does not affect the generality of the coherent control method discussed in this study. The gold nanowire has a radius of 50 nm and is surrounded by air. It is excited by a low-intensity field of wavelength $\lambda = 532$ nm (the signal) and by a second high-intensity field of wavelength 2λ (the control). We are interested in the properties of light radiated at λ. When the nanowire is excited by the signal beam only, the optical response is characterized by an electric dipole pointing along the x axis. The left panel of Fig. 2(a) provides a sketch of the near-field charge distribution. It has an odd symmetry, with two poles defining the electric field lines. The right panel of Fig. 2(a) shows the corresponding radiation pattern. It features two lobes pointing forwards ($\theta = 90°$) and backwards ($\theta = 270°$). A different situation is encountered if the nanowire is excited by SHG, that is, by the control beam [Fig. 2(b)]. The charge distribution now has even parity (left panel) with radiation lobes that are directed towards the same side (right panel). As discussed before, SHG in metal nanostructures has different origins and our model takes both nonlinear dipole and quadrupole terms into account, that is, Fig. 2(b) is the result of both terms.

Next, we excite the gold nanorod by both the signal field and the control field [Fig. 2(c)]. The interference between the two terms gives rise to an asymmetric polarization charge distribution (left panel) and an asymmetric radiation pattern (right panel). For a pronounced effect, the contributions from signal and control must be of similar magnitude. For the gold nanorod considered here we adjust the excitation fields of signal and control as $\mathbf{E}_{\text{control}} = \alpha \mathbf{E}_{\text{signal}}$, where $\alpha \sim 10^5 \exp(i\delta\pi)$. The results shown in Fig. 2(c) have been calculated for zero phase delay ($\delta = 0$) and it is evident that the charge distribution and the radiation pattern will depend on δ. The asymmetry in the radiation pattern shown in Fig. 2(c) is a consequence of retardation. Note that the excitation fields $\mathbf{E}_{\text{signal}}$ and $\mathbf{E}_{\text{control}}$ have different frequencies and that their phases need to be locked.

We now investigate the influence of δ on the directionality and the intensity of scattered light at wavelength λ. Figure 3(a) shows the radiation patterns for three different phase delays. From these far-field maps we calculate the directionality, defined as the ratio of maximum intensity emitted to the left to maximum intensity emitted to the right. As shown in Fig. 3(b), the directionality can be tuned over 4 orders of magnitude by varying the phase delay δ.

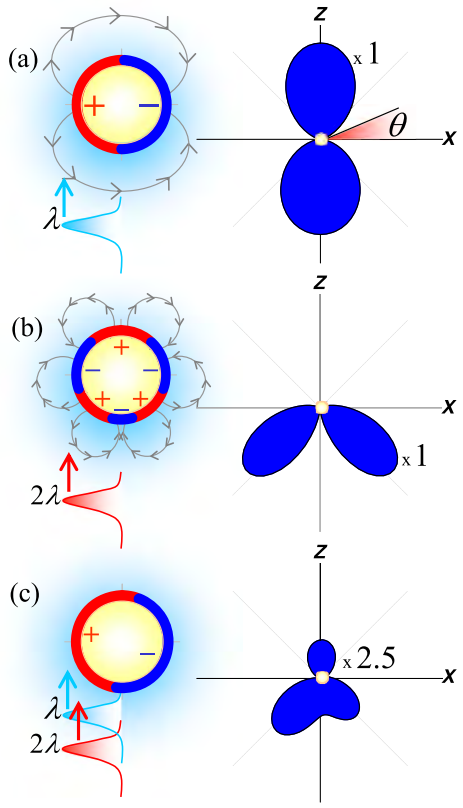

FIG. 2 (color online). Charge distributions (left) and radiation patterns (right) of a gold nanowire excited under different conditions. (a) Linear scattering of a signal beam of wavelength λ. (b) Second-harmonic generation with a control beam of wavelength 2λ. (c) Excitation by both signal and control beams. The linearly scattered signal field and the second-harmonic control field interfere and give rise to an asymmetric charge and radiation pattern.

Figure 3(c) shows the radiation efficiency as a function of δ, defined as the total scattered power in the presence of both signal and control beams normalized with the scattered power in absence of the control plus the scattered power in absence of the signal. The curve indicates that the radiation efficiency is not affected by the phase delay. In other words, δ influences the directionality but leaves the total area covered by the radiation patterns unaffected. The ability to steer the radiation with a dynamic range of 4 orders of magnitude without introducing any losses is unique. Similar results are traditionally achieved with phased-array antennas, or with multielement antennas (e.g., Yagi-Uda) but with a considerably larger footprint and complexity. Note that the nanowire considered here is not an optimized geometry and that much stronger effects can be achieved with suitably designed antennas [24].

Interestingly, we can find excitation conditions for which the total scattered power can be suppressed or enhanced. To demonstrate such a situation we excite the

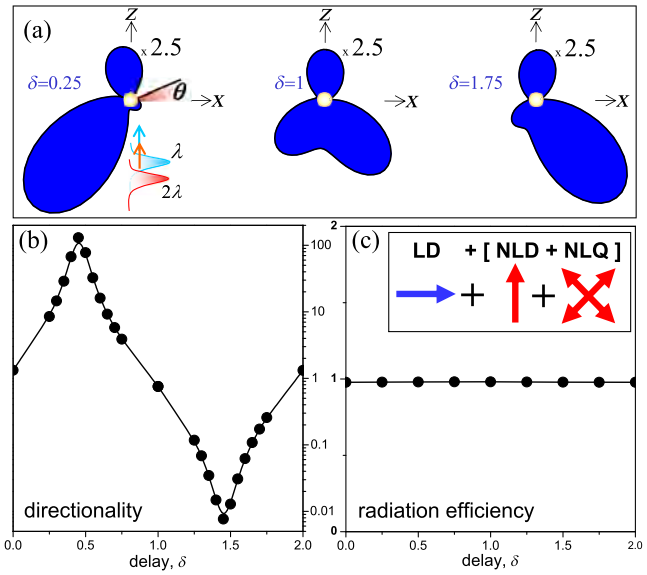

FIG. 3 (color online). Control of radiation efficiency and directionality by phase delay δ. Signal and control beams are collinear. (a) Radiation patterns for three different δ. (b) Directionality as a function of δ. (c) Normalized total scattered power as a function of δ. See main text for definitions. The arrows in the inset represent the induced linear dipole (LD), nonlinear dipole (NLD), and nonlinear quadrupole (NLQ).

antenna with orthogonal beams, that is, control and signal beams are incident from angles that differ by 90 degrees. As shown in Figs. 4(a) and 4(b), this configuration has almost no effect on the directionality. The radiation pattern remains symmetric for all phase delays δ. However, the area of the radiation patterns and hence the radiation efficiency changes drastically [Fig. 4(a)]. While the large area of the "fly"-like pattern at $\delta = 0.5$ rapidly reduces when increasing the phase delay to $\delta = 1.5$, the directionality remains unaltered. In contrast, the radiation efficiency oscillates sinusoidally, reaching values either larger or smaller than one [see Fig. 4(c)]. Thus, depending on the phase delay and the angles of incidence we are able to suppress or enhance light scattering. The reason why light scattering can be suppressed is that an induced charge density can be generated having a negligible dipole component, that is, the charge distribution corresponds to a dark mode [25–29].

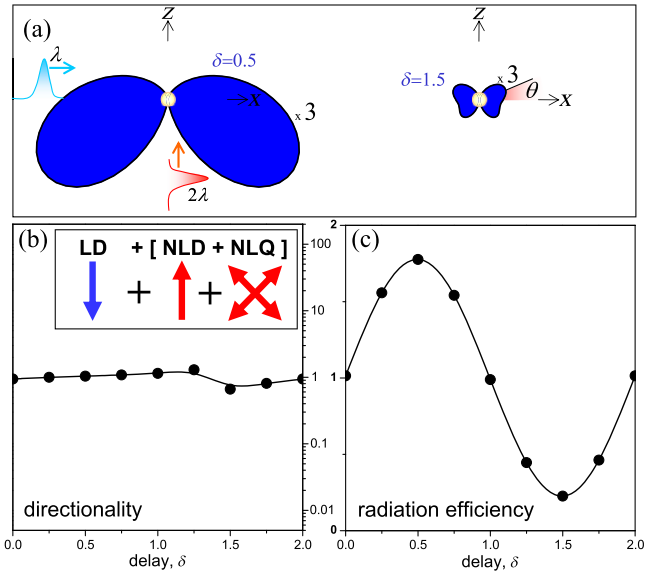

FIG. 4 (color online). Similar study to the one shown in Fig. 3, but with signal and control beams aligned orthogonally.

To better understand why in the collinear case the phase delay δ only affects the directionality (Fig. 3) and in the orthogonal case it only affects the radiation efficiency (Fig. 4) we perform calculations as a function of the angle φ between the incident beams. For this purpose we keep the control beam angle fixed (normal incidence) and adjust the phase delay to $\delta = 0.5$. The calculated radiation efficiency, shown in Fig. 5, exhibits a complicated behavior with peaks and dips, which arise from the interactions between the different $\chi^{(2)}$ contributions, namely the linear and nonlinear dipole interactions and the quadrupole interaction. To illustrate the contribution of the quadrupole term we implemented a simple model of two interacting dipoles (one of them fixed, the other being rotated with angle φ). This model accounts for the interaction between the linear dipole mode and the nonlinear dipole mode [30,31]. The result is shown as the thick red curve in Fig. 5. Evidently, constructive and destructive dipole-dipole interactions cannot explain our results, the disagreement being most pronounced for angles $\varphi = 135°$ and $\varphi = 315°$ (see blue shaded areas in Fig. 5). While for $\varphi = 135°$ the dipole-dipole response and the full calculation display similar radiation patterns, the corresponding radiation efficiencies are markedly different: the dipole-dipole model predicts

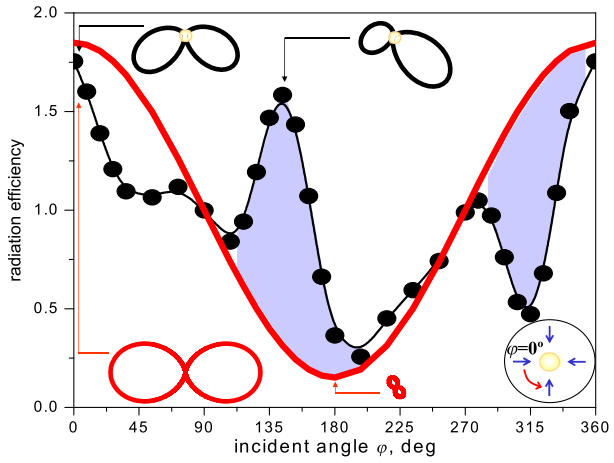

FIG. 5 (color online). Radiation efficiency as a function of the signal beam incidence angle, $\delta = 0.5$. The solid thick red line represents the calculated far-field efficiency of two interacting electric dipoles (see text for details).

attenuation whereas the full calculation yields an enhancement of the radiation efficiency. For $\varphi = 315°$ we find the opposite scenario. Thus, the coherent control mechanism exploited in this work depends on the specific symmetry of the second-order nonlinear susceptibility and on the relative magnitude of its components. In Fig. 3, the control beam breaks the charge symmetry induced by the signal beam, but the induced modes (linear dipole, nonlinear dipole, and quadrupole) remain orthogonal. This is the reason why the radiation efficiency is not affected by the phase delay δ. For the situation in Fig. 4, on the other hand, the linear dipole and the nonlinear dipole are *not* orthogonal, which means that the total dipole moment can be enhanced or suppressed, thereby affecting the radiation efficiency. None of the results involving quadrupole fields are achievable with a purely *linear* scattering approach [32,33]. A true dark mode cannot be excited by linear excitation; however, it can be excited through SHG [34]. In practice, retardation effects make it possible to excite quadrupole modes even with linear excitation, especially for larger particle sizes. However, SHG provides a means for much more efficient excitation of dark modes [34].

In conclusion, we introduced a method for coherent control of light scattering by nanoparticles. A control beam "writes" a polarization charge distribution into the scattering object via SHG, whereas a signal beam then interacts with this charge distribution. The coherent interaction between SHG from the control beam and linear scattering from the signal beam gives rise to directional radiation. The directionality and radiation efficiency can be tuned by varying the phase delay δ between control and signal beams. The theoretical results presented in this work can be experimentally tested using standard pump-probe spectroscopy with a fixed phase relation between pump and probe pulses. Experimentally, a homogeneous environment can be achieved by depositing nanoparticles on a dielectric substrate and using index matching liquids for coverage. The concept developed here is neither limited to simple geometries nor metallic materials. The work opens the door for engineering the surface charge density of nanostructures, which can be employed in spectroscopy when nondipolar transitions take place [35], and for sensing using localized surface plasmon resonances [34].

This work was funded by the U.S. Department of Energy (Grant No. DE-FG02-01ER15204). S. G. R. is thankful for support from the Spanish "Ministerio de Educación" under grant "Programa Nacional de Movilidad de Recursos Humanos del Plan Nacional de I-D+i 2008-2011."

[1] S. A. Maier, *Plasmonics: Fundamentals and Applications* (Springer, Berlin, 2007).
[2] S. I. Bozhevolnyi, *Plasmonic Nanoguides and Circuits* (Pan Stanford Publishing, Singapore, 2009).
[3] H. A. Atwater and A. Polman, Nat. Mater. **9**, 205 (2010).
[4] H. Harutyunyan, G. Volpe, R. Quidant, and L. Novotny, Phys. Rev. Lett. **108**, 217403 (2012).
[5] L. Novotny and N. F. van Hulst, Nat. Photonics **5**, 83 (2011), and references therein.
[6] M. W. Knight, H. Sobhani, P. Nordlander, and N. J. Halas, Science **332**, 702 (2011).
[7] A. G. Curto, G. Volpe, T. H. Taminiau, M. P. Kreuzer, R. Quidant, and N. F. van Hulst, Science **329**, 930 (2010).
[8] E. C. Hao, G. C. Schatz, R. C. Johnson, and J. T. Hupp, J. Chem. Phys. **117**, 5963 (2002).
[9] S. I. Bozhevolnyi and V. Z. Lozovski, Phys. Rev. B **65**, 235420 (2002).
[10] J. Shan, J. I. Dadap, I. Stiopkin, G. A. Reider, and T. F. Heinz, Phys. Rev. A **73**, 023819 (2006).
[11] S. Palomba and L. Novotny, Phys. Rev. Lett. **101**, 056802 (2008).
[12] A. K. Singh, D. Senapati, A. Neely, G. Kolawole, C. Hawker, and P. C. Ray, Chem. Phys. Lett. **481**, 94 (2009).
[13] G. Bachelier, J. Butet, I. Russier-Antoine, C. Jonin, E. Benichou, and P.-F. Brevet, Phys. Rev. B **82**, 235403 (2010).
[14] J. Butet, G. Bachelier, I. Russier-Antoine, C. Jonin, E. Benichou, and P.-F. Brevet, Phys. Rev. Lett. **105**, 077401 (2010).
[15] J. Butet, J. Duboisset, G. Bachelier, I. Russier-Antoine, E. Benichou, C. Jonin, and P.-F. Brevet, Nano Lett. **10**, 1717 (2010).
[16] P. A. Franken, A. E. Hill, C. W. Peters, and G. Weinreich, Phys. Rev. Lett. **7**, 118 (1961).
[17] A. Taflove and S. C. Hagness, *Computational Electrodynamics: The Finite-Difference Time-Domain Method* (Artech House, Boston, 2005), 3rd ed.
[18] L. Novotny and B. Hecht, *Principles of Nano-Optics* (Cambridge University Press, Cambridge, England, 2006), Chap. 15.
[19] S. G. Rodrigo, F. J. García-Vidal, and L. Martín-Moreno, Phys. Rev. B **77**, 075401 (2008).
[20] J. E. Sipe, V. C. Y. So, M. Fukui, and G. I. Stegeman, Phys. Rev. B **21**, 4389 (1980).
[21] P. Guyot-Sionnest, W. Chen, and Y. R. Shen, Phys. Rev. B **33**, 8254 (1986).
[22] F. X. Wang, F. J. Rodríguez, W. M. Albers, R. Ahorinta, J. E. Sipe, and M. Kauranen, Phys. Rev. B **80**, 233402 (2009).
[23] K. A. O'Donnell and R. Torre, New J. Phys. **7**, 154 (2005).
[24] M. Finazzi, P. Biagioni, M. Celebrano, and L. Duò, Phys. Rev. B **76**, 125414 (2007).
[25] M. I. Stockman, S. V. Faleev, and D. J. Bergman, Phys. Rev. Lett. **87**, 167401 (2001).
[26] N. Liu, L. Langguth, T. Weiss, J. Kästel, M. Fleischhauer, T. Pfau, and H. Giessen, Nat. Mater. **8**, 758 (2009).
[27] J. A. Fan, C. Wu, K. Bao, J. Bao, R. Bardhan, N. J. Halas, V. N. Manoharan, P. Nordlander, G. Shvets, and F. Capasso, Science **328**, 1135 (2010).
[28] B. Luk'yanchuk, N. I. Zheludev, S. A. Maier, N. J. Halas, P. Nordlander, H. Giessen, and C. T. Chong, Nat. Mater. **9**, 707 (2010).
[29] J.-S. Huang, J. Kern, P. Geisler, P. Weinmann, M. Kamp, A. Forchel, P. Biagioni, and B. Hecht, Nano Lett. **10**, 2105 (2010).

[30] J. I. Dadap, J. Shan, K. B. Eisenthal, and T. F. Heinz, Phys. Rev. Lett. **83**, 4045 (1999).
[31] J. I. Dadap, J. Shan, and T. F. Heinz, J. Opt. Soc. Am. B **21**, 1328 (2004).
[32] M. Liu, T.-W. Lee, S. K. Gray, P. Guyot-Sionnest, and M. Pelton, Phys. Rev. Lett. **102**, 107401 (2009).
[33] T. H. Taminiau, F. D. Stefani, and N. F. van Hulst, Nano Lett. **11**, 1020 (2011).
[34] J. Butet, I. Russier-Antoine, C. Jonin, N. Lascoux, E. Benichou, and P.-F. Brevet, Nano Lett. **12**, 1697 (2012).
[35] J. Kwela, Z. Phys. D **13**, 101 (1989).